Spatial distribution of polyelectrolyte and counterions in nanocapsules: A computer simulation study

Mikhail R. Stukan,[1] Vladimir Lobaskin,[1,2] Christian Holm,[1,3] and Olga I. Vinogradova[1,4]
[1]*Max Planck Institute for Polymer Research, Ackermannweg 10, 55128 Mainz, Germany*
[2]*Physics Department, Technical University of Munich, 85747 Garching, Germany*
[3]*Frankfurt Institute for Advanced Studies, Johann Wolfgang Goethe University, Max-von-Laue-Strasse 1, 60438 Frankfurt am Main, Germany*
[4]*A. N. Frumkin Institute of Physical Chemistry and Electrochemistry, Russian Academy of Sciences, 31 Leninsky Prospect, 119991 Moscow, Russia*
(Received 30 August 2005; published 27 February 2006)

We study a spatial distribution of polyelectrolyte chains and counterions inside nanometer-size capsules by means of molecular dynamics simulation on the level of a colloidal model in which polyelectrolyte coils are modeled as soft charged spheres. The capsule shell is treated as a semipermeable membrane, impermeable for the polyelectrolyte chains, but allowing free diffusion of solvent molecules and counterions. As a result, counterions leak out from the capsule immersed into a fluid of low ionic strength. This counterion leakage leads to a formation of characteristic polyelectrolyte density profiles with the central plateau and large peaks at the wall. We show that a nonuniform distribution of the inner polyelectrolyte depends on the capsule radius, surface charge, concentration of encapsulated polyelectrolyte, and the volume fraction of capsules.

DOI: 10.1103/PhysRevE.73.021801 PACS number(s): 82.35.Rs, 61.20.Ja, 82.20.Wt

I. INTRODUCTION

In recent years, there has been much interest in studying polyelectrolyte multilayer micro and nanocapsules, mostly "hollow" [1,2], but also filled with a solution of a charged polymer. Such "filled" capsules can be prepared by a variety of methods [3–7] and represent a type of nanoengineered composites, potentially important in many areas of science and technology. For instance, they allow one to mimic advanced systems containing biopolymers, perhaps even living cells, and could serve as a new hybrid material with controlled stiffness [8–10].

The multilayer shell of such capsules represents a semipermeable membrane, being impermeable to high molecular weight compounds, but allowing diffusion of solvent molecules and/or small counterions [11,12]. As a result, rich osmotic and electrostatic equilibria for encapsulated polyelectrolytes are possible, which makes properties of "filled" capsules essentially different from all other systems studied before, including those of "hollow" capsules. In particular, the counterion release could dramatically change the mechanical and interaction properties of capsules, as well as the spatial distribution of encapsulated materials. However, modern optical methods (e.g., a confocal scanning microscopy) allow only measurements of the distribution of (fluorescently labeled) macromolecules or nanoparticles, but not of the counterions. Moreover, optical methods are limited to studying quantitatively only relatively large capsules, whose characteristic sizes exceed the wavelength (of the order of 500 nm) of the source of light used to excite the fluorescence signal. Therefore, they are not suitable for studying the distribution of an encapsulated material inside nanocapsules, and do not allow one to draw definite conclusions concerning its adsorption on the nanoshell (normally approximately 10 nm thick). The lack of experimental information could partly be compensated by computer simulation of the corresponding model system. The purpose of the present paper is to study by means of molecular dynamics (MD) the distribution of charged encapsulated material and counterions, typical for a nanocapsule with a semipermeable shell. As an initial application of our approach we have chosen to investigate capsules containing polyelectrolyte chains immersed in a salt-free solution. Extensions of our method to study other systems would be straightforward.

Our paper is arranged as follows. In Sec. II we formulate the so-called colloidal model describing a nanocapsule with encapsulated polyelectrolyte chains. In our approach, polyelectrolyte chains are modeled as charged soft spheres capable of interpenetration. A justification of our coarse-grained model and the evaluation of its parameters were done by performing the simulation of polyelectrolyte solution in the bulk. The results of the simulation of "filled" polyelectrolyte capsules are highlighted in Sec. III. Our main results are that a significant leakage of counterions from the capsule interior is possible depending on the volume fraction of capsules, charge, and concentration of encapsulated polymer chains. This counterion leakage leads to a nonuniform spatial distribution of inner charged polymer chains. In addition to a central plateau region, the polyelectrolyte density profiles show large adsorption peaks at the wall, in agreement with experimental observations [11,12]. We conclude in Sec. IV.

II. MODEL

A. General consideration

For the sake of brevity, only a short description of the model and main ideas is given here. Our key idea is to mimic a spatial distribution of polyelectrolyte chains inside the capsule by using the so-called colloidal model. In a quite general framework, the positions of a monomer in a polymer solu-

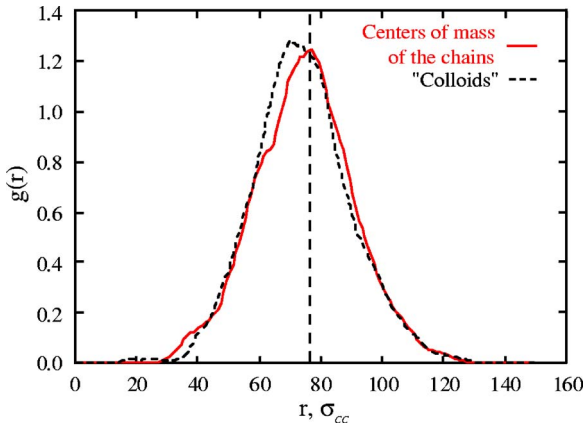

FIG. 1. (Color online) Pair distribution function for the centers of mass of polymer chains in the bulk as obtained from the MD simulation of the bead-spring model and the same distribution obtained from MD simulation of the "colloidal" model. The vertical dashed line shows the half of the simulation box.

tion $\vec{r}$ can be represented in terms of the position of the chain's center of mass $\vec{r}^{cm}$ plus the monomer displacement relative to the center of mass of the corresponding chain, $\vec{r}_i = \vec{r}_k^{cm} + (\vec{r}_i - \vec{r}_k^{cm})$, where i indicates the monomers belonging to one chain and k is the index of the chain. In dilute polyelectrolyte solutions the spatial distribution of monomers is dominated by the distribution of centers of mass of polyelectrolyte chains, which are well separated in space due to Coulomb repulsion between the like-charged chains, $\vec{r}_k^{cm} - \vec{r}_l^{cm} \gg (\vec{r}_i - \vec{r}_k^{cm})$, k,l being the indices of different chains. They can therefore be treated as separate entities, while the influence of the precise chain conformation on this distribution of polyelectrolyte chain can be neglected. Briefly, we suggest the treatment of each polymer coil as a soft sphere of radius R_{poly}. Then the charge of such an equivalent spherical particle is equal to a sum of charge of a polyelectrolyte and counterions confined within a distance of R_{poly} from the center of mass of the chain. The remaining counterions are considered explicitly and are excluded from the core by means of a soft repulsive potential. We further allow polymer-polymer pairs to interpenetrate. For dilute solutions, where polymer coils do not overlap or overlap weakly, it is possible to chose parameters for the model in such a way that the pair distribution function of "colloidal" polymer particles coincides with that of centers of mass of polymer chains in the "full" simulation (see Fig. 1). We are unaware of any previous work that has modeled polyelectrolyte chains in such a way, although a similar strategy was used for colloid-polymer mixtures [13,14], dilute solutions of neutral polymer coils [15,16], star polymers [17], and microgel particles [18].

The multilayer shell is modeled as a spherical wall constraint. In other words we consider the shell to be an infinitesimally thin, neutral, and rigid interface. These assumptions, made in order to simplify the analysis, are justified provided that the shell thickness is much smaller than the radius of the capsules, the multilayer charge is negligible as compared with that of the inner solution, and the degree of capsule swelling caused by an excess inner osmotic pressure is small. Our simplifications are therefore consistent with known experimental parameters and facts [11]. The selective permeability of the shell is tuned by introducing the repulsive interaction with the polymer entities only, which allows us to make it impermeable for polymers but permeable for counterions. The total simulation volume is restricted by spherical constraint impermeable for counterions. Thus, by changing the radii of these external and "capsules" constraints, we can vary the volume fraction of capsules in solution.

B. Bulk simulation

Our reference system for tuning the parameters of the equivalent dispersion of soft spheres to the properties of a polyelectrolyte solution is represented on the level of a primitive model. We aim to reproduce the spatial distributions of the chains as well as the counterions of the standard system, which represents a polyelectrolyte solution inside a multilayer capsule.

In the reference system, polyelectrolyte chains were modeled as bead-spring chains of Lennard-Jones (LJ) particles. Excluded volume interactions between all monomer units as well as counterions were emulated by a repulsive Lennard-Jones (RLJ) potential with the cutoff $r_c = 2^{1/6}\sigma$,

$$U_{LJ}(r) = \begin{cases} 4\varepsilon\left[\left(\frac{\sigma}{r}\right)^{12} - \left(\frac{\sigma}{r}\right)^{6} - \left(\frac{\sigma}{r_c}\right)^{12} + \left(\frac{\sigma}{r_c}\right)^{6}\right], & r \leqslant r_c, \\ 0, & r > r_c. \end{cases} \tag{1}$$

The units of length and energy in all presented data were set by σ and ε, respectively (LJ units). The energy parameter ε controls the strength of the interaction, and its value was fixed to $\varepsilon = 1.0 k_B T$, where k_B is the Boltzmann constant and T is the temperature. The counterion-counterion and monomer-monomer interaction radii were scaled by σ_{cc} and σ_{mm} ($\sigma_{cc} = \sigma_{mm} = 1$), respectively [see Eq. (1)], and the counterion-monomer radius was a fitting parameter in the simulation. Below we describe the criteria used for its selection.

The monomer units of the model chains were connected by finitely extensible nonlinear elastic (FENE) bonds,

$$U_{\text{FENE}}(r) = -\frac{1}{2} k R_0^2 \ln\left(1 - \frac{r^2}{R_0^2}\right). \tag{2}$$

The spring constant k and the maximum extension of the bond, R_0 [see Eq. (2)] were chosen as $k = 27 k_B T/\sigma^2$ and $R_0 = 2\sigma$. For such values the average distance between monomer units along the chain was $\langle l_{bond} \rangle = 1 \pm 0.01$.

Within the primitive model, the electrostatic interaction is given by the Coulomb potential

$$U_{\text{Coul}}(r_{ij}) = k_B T \frac{\lambda_B q_i q_j}{r_{ij}}, \tag{3}$$

where $q_i = -1$ for the charged chain monomers and $q_i = +1$ for the counterions, and the Bjerrum length

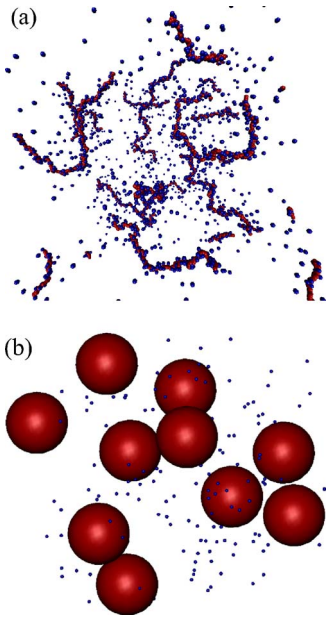

FIG. 2. (Color online) Snapshots from an MD simulation of polyelectrolyte molecules in the bulk (a) and corresponding "colloidal" system (b).

$$\lambda_B = \frac{e^2}{4\pi\varepsilon_S\varepsilon_0 k_B T}, \tag{4}$$

where e is the elementary charge, and ε_0 and ε_S are the dielectric constant of vacuum and the relative dielectric constant of the solvent, respectively.

As a reference experimental system in our simulation we used aqueous solution of polystyrene sulfonate (PSS). The Bjerrum length in water at 298 K is equal to 7.14 Å, which gives $\lambda_B = 2.65 \approx 7.14/2.68$ in our LJ units (the length of a PSS monomer unit is 2.68 Å). We studied a bulk solution with number density of polyelectrolyte $2.63 \times 10^{-6}\sigma^{-3}$. To estimate finite size effects we considered systems of 10 or 20 fully charged polymer chains (each monomer unit of the chain has valence $q=-1$), which consisted of 220 monomer units each in a cubic simulation box with periodic boundary conditions. The sizes of the simulation boxes were 156 ($58.65\lambda_B$) and 197 ($74.06\lambda_B$) for the case of 10 and 20 polyelectrolyte molecules respectively, according to the chosen number density of polyelectrolyte. Molecular dynamics with the Langevin thermostat at temperature 298 K was used. The long-range Coulomb interactions were treated using the Particle-Particle-Particle-Mesh algorithm [19] in the implementation of [20]. Simulations were performed using the ESPResSo molecular simulation package [21,22].

The Lennard-Jones radius of the monomer-counterion interaction σ_{mc} was tuned to reproduce the value of osmotic coefficient ϕ known from the experiments on aqueous PSS solutions [23–26] ($C_{\mathrm{PSS}}=0.05$ monomol/L, salt-free solution, $\phi \sim 0.17-0.2$). The required osmotic coefficient ($\phi \leq 0.2$) was obtained at $\sigma_{mc}=1$ (ϕ was equal to 0.18 for 10 and to 0.17 for 20 PSS chains respectively).

The studied polymer chains in the bulk take horseshoe and double-horseshoe conformation [see. Fig. 2(a)] and their characteristic parameters for the case of 10 chains in the box are: radius of gyration $\langle R_g\rangle_{10}=27.7$, end-to-end distance $\langle R_e\rangle_{10}=73.5$, characteristic ratio $a=\langle R_e^2/R_g^2\rangle_{10}=7$; for the case of 20 chains in the box: $\langle R_g\rangle_{20}=26.1$, $\langle R_e\rangle_{20}=69.9$, $a=\langle R_e^2/R_g^2\rangle_{20}=7$. They are in a good agreement for both system sizes, so that one can conclude that finite size effects do not influence our results. The radius of gyration corresponds to the experimental results (for PSS 5–6 nm). The pair distribution function $g(r)$ of the centers of mass of polymers is shown in Fig. 1 [during bulk simulation runs we used the following criteria of equilibration—the system was treated as an equilibrated one if the profiles of $g(r)$ as well as values of R_g, R_e, l_{bond} obtained in two consequent runs of 10^6 MD steps (integration step was 0.01 LJ time units) coincide].

Based on the results of the bulk simulation, we evaluated parameters of the colloidal model of the polyelectrolyte solution. Effective radius and effective charge of soft spherical polymer particles was chosen in such a way that the pair distribution function $g(r)$ of these spheres coincides with that of the centers of mass of the chains in the bulk. The best fit was reached for $R_p=26\pm1, Q_p=15\pm1e$ (see Fig. 1). This effective radius of the colloidal coil is very close to the radius of gyration of polymer chains in the bulk. Taking into account the value of characteristic ratio a ($a\approx7$) we can conclude that the conformations of our molecules are close to those obtained by self-avoiding walk ($a_{SAW}=6.3$). In other words, the chains in our study are long in comparison with the electrostatic persistence length {the Odijk-Skolnick-Fixman electrostatic persistence length [27,28] for this chain is $l^{OSF}=\lambda_B/(2\kappa\sigma_{mm}/\phi)^2 \approx 40$ or 0.18 of the chain contour length}, so that the approximation of polymer coils as spherical objects is justified. The final coarse-grained system is the following. Polymer coils as well as remaining counterions are treated as Lennard-Jones particles with charge $Q_p=-15e$ and $q=-1e$, respectively. The renormalized charges and ions are still treated within the primitive model [the interactions between particles are determined by Eq. (1)]. Interaction radii are $\sigma_{pc}=25$ polymer-counterion, $\sigma_{cc}=1$ counterion-counterion, $\sigma_{pp}=5$ polymer-polymer, so "polymer coils" in our model can "overlap" due to very soft interaction between them (the Coulomb potential) but free counterions cannot go inside the "polymer coils." Thus, the effective coil size can be interpreted only in the sense of ion exclusion from the effective particle core. Note that at the chosen conditions it is impossible to recover completely the "wings" of the counterion distribution (though sizes of the ionic cloud (the distance at which the accumulated charge turns to zero) coincide in the colloidal and bead-spring models) and simultaneously reproduce the center-of-mass distribution since effective pair interactions between the polyions is nonadditive [29,30]. Therefore, this model might produce a systematic shift in either prediction of the counterion distribution or the coil distribution. Another careful study of the distributions would be needed to see whether these shifts could be minimized by a proper choice of the coil-ion potential. For this work, we decided to fix rather the coil distribution to facilitate the comparison to the available experimental data (from the confocal fluorescence microscopy).

The shell and polymer particles interact according to the repulsive Lennard-Jones potential [Eq. (1)], as the simplest

one, with interaction radii $\sigma_{ps}=1$. Although the model of the capsule does not take into account the shell structure and possible net charge, the simplification affects only the polymer and counterion distributions near the wall. The net charge on the shell changes the distribution of the electrostatic potential and therefore the equilibrium between the inner capsule volume and the bulk. Our calculations, however, show that the effective surface charge density of the shell itself in this case is small in comparison to the "induced" charge density due to polymer encapsulation.

III. RESULTS AND DISCUSSION

By using the colloidal model described above, we simulated filled capsules of three differen radii: 250, 300, and 350 σ_{cc} (67 nm, 80 nm, and 94 nm). For each capsule size we have considered the following number densities of encapsulated substance $C=1.77\times10^{-6}$, 2.65×10^{-6}, and 3.54×10^{-6}. For the capsule size $R=300\sigma_{cc}$ we additionally modeled systems with number densities of encapsulated material equal to 1.54×10^{-6} and 2.04×10^{-6}. Although in reality there is always some amount of background ions due to water dissociation or presence of carbon dioxide, in the range of about 1×10^{-5} to 1×10^{-6} mol/L, this does not play a major role for our concentrated capsule dispersions and we therefore considered a salt-free system. For the most dilute regime 1.77×10^{-6} and the largest external volume $R_{ext}=1000\sigma_{cc}$, the number of counterions at the center the capsule changes by about 3% [from 1752 (no salt) to 1814 (salt concentration 1×10^{-5} mol/L)]. The detailed study of the influence of salt on the polymer distribution and counterion leakage is currently in progress and will be published at a later date. Although the variation of the concentration affects the effective radius and the charge of polyelectrolyte coils, the difference does not exceed 3%, so we used the same parameters of the colloidal model at all conditions.

It is known from experiment [9,10] that the polyelectrolyte density profile inside the capsule changes with the polyelectrolyte concentration. The appearance of maxima in the polymer distribution profile at the wall suggests that repulsions between the charged polymer coils are not completely screened. Indeed, these maxima were not observed for encapsulated neutral polymers [31]. One can, therefore, suppose that a certain fraction of the counterions escapes from the capsule interior into the bulk solution, and that this fraction is getting larger upon dilution of the dispersion of capsules. We studied the dependence of the polymer density profile on capsule volume fraction using a spherical Wigner-Seitz (WS) cell model. The radius of the simulation cell and hence its volume, V_{cell} were varied. The "external" volume (volume outside the "capsule" available for counterions only) influences the number of counterions inside the capsule for entropic reasons. The surface charge density of the capsule due to the counterion leakage as a function of the capsule volume fraction $\Phi=V_{caps}/V_{cell}$ is shown in Fig. 3. One can see that in case $\Phi=1$, the capsule is neutral since the total negative charge of polyelectrolyte chains is compensated by a corresponding number of counterions inside the capsule. With the decrease in the capsule volume fraction,

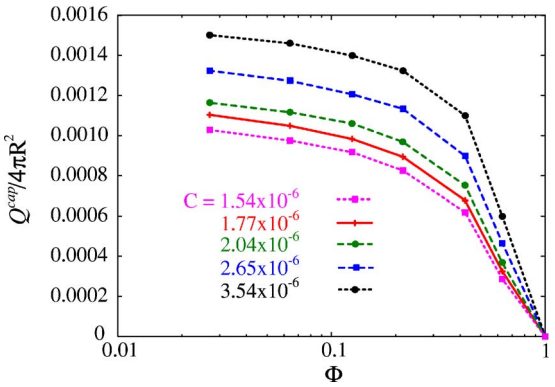

FIG. 3. (Color online) Effective surface charge density of the capsule, $Q^{cap}/4\pi R^2$, as a function of the capsule volume fraction, Φ for different concentrations of encapsulated polyelectrolyte, C (capsule radius $R=300\sigma_{cc}$).

the effective surface charge density of the capsule increases. For small Φ this dependence is logarithmic, although in a real experiment it rather tends to a constant value due to the presence of background ions. Nevertheless, as we mentioned above, in the range of parameters used here, the "salt-free" approximation is rather accurate.

The ion leakage from the capsule can be characterized by the apparent charge density of the capsule surface, which is defined by the relation of the net charge of the filled capsule to the shell surface area. We included in Q^{cap} all the charged particles inside the capsule and the counterions "associated" with it, i.e., residing in the thin layer ($\Delta R=26=\sigma_{pc}$) outside the capsule surface (these counterions we presume to be condensed at the polymer coils). This definition of the charge takes into account the ionic condensation on a charged shell and thus allows one to estimate the effective renormalized charge of the capsule, the value that one could observe experimentally in electrophoretic measurements or while studying of capsule interactions or distribution in the dispersion [32,33]. The effective charge densities obtained for the capsules of radius $300\sigma_{cc}$ with different concentrations of encapsulated polyelectrolyte, C, are shown in Fig. 3. Capsules of other radii show similar trends. Moreover, as one can see from Fig. 4, for relatively low concentration of capsules the effective surface charge density does not depend on the radius of the capsule and remains constant for a given concentration of encapsulated polyelectrolyte C and capsule volume fraction Φ. One can say therefore that scaling the system up preserves the surface density of polymer chains in the layer adjacent to the capsule wall due to conservation of the electrochemical balance between the ions inside the capsule and in the bulk solution. This observation is crucial. It suggests that our results can be used to estimate the charge of capsules of an arbitrary size provided that the capsule volume fraction and the polyelectrolyte concentration are given.

Figure 5 shows how does the counterion density profile depend on the concentration of encapsulated polyelectrolyte, capsule radius, and volume fraction of capsules in the system with capsule concentration Φ. All counterion density profiles look similar. Namely, they are flat in the capsule interior except of the narrow layer close to the shell, where a small, but discernible, peak appears. The existence of a small peak

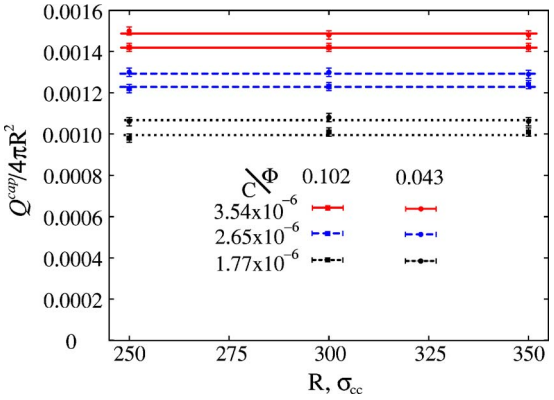

FIG. 4. (Color online) Effective surface charge density, $Q^{cap}/4\pi R^2$ as a function of capsule radius, R, for different concentrations of encapsulated polyelectrolyte, C, and capsule volume fraction, Φ.

near the wall is due to association of counterions with the adsorbed charged polymer chains (see below). The counterion concentration inside the capsule increases with either of (i) the volume fraction Φ, (ii) the capsule radius R at a fixed volume fraction, or (iii) the polyelectrolyte concentration inside the capsule. The outer wings of the distribution peaks display also a shoulder with an inflection point at the capsule wall position. The inflection point indicates the junction of two qualitatively different ionic distributions: the one inside the capsule, which is strongly influenced by the polymer density profile, and the distribution in the bulk solution, which is governed by the surface potential of the charged capsule. Note that a difference between counter-ions densities in the central plateau and in the bulk potentially allows us to evaluate the contribution of counter-ions to the excess inner osmotic pressure [via $\Pi_{ion}=(\rho_{in}-\rho_{out})k_BT$]. The exact calculation of the inner osmotic pressure and pressure exserted by the shell remains an open question for future study. However, already from the curves presented in Fig. 5(b) one can conclude that the contribution of counterions to the inner osmotic pressure significantly decreases with the decrease in the capsule radius. Note, however, that an excess osmotic pressure in the center of capsules is not equal the pressure exserted by the shell. This in particular means that the theoretical model developed for evaluation of osmotic swelling of impermeable for counter-ions capsules [6] should be modified in case of capsules with semi-permeable shells by taking into account the counter-ion leakage and a contribution of polymer chains to the contact pressure.

Let us now discuss how the main system parameters (capsule radius, cell size, and concentration of encapsulated material) influence the distribution of polyelectrolyte inside the capsule. First of all, the leakage of counterions out of the capsule leads to the buildup of a noncompensated polymer charge and this leads to a formation of a density peak near the capsule wall due to repulsive interactions (see Fig. 5). To quantify this effect we have considered the ratio $\hat{\rho}/\bar{\rho}$, where $\bar{\rho}$ is the average density of polyelectrolyte inside the capsule and $\hat{\rho}$ is the average density of polyelectrolyte inside the peak near the wall (averaging is performed inside the surface layer with the width of $25\sigma_{cc}$)(see Fig. 6). Note some qualitative similarity to the data on charge densities. Thus, the same logarithmic dependence appears at low concentrations of capsules. However, in contrast to the results of the charge density of the capsules, the polyelectrolyte distribution profiles contain an intersection point at $\Phi \approx 0.65$. Physically, this is caused by the fact that at large values of Φ the depletion effect near the shell is stronger for low concentrations of polyelectrolyte, while for low Φ ratio $\hat{\rho}/\bar{\rho}$ is higher. Unfortunately, relatively small range of radii used in our simulation does not allow us to make any definite conclusion about the dependence of this parameter on the capsule radius.

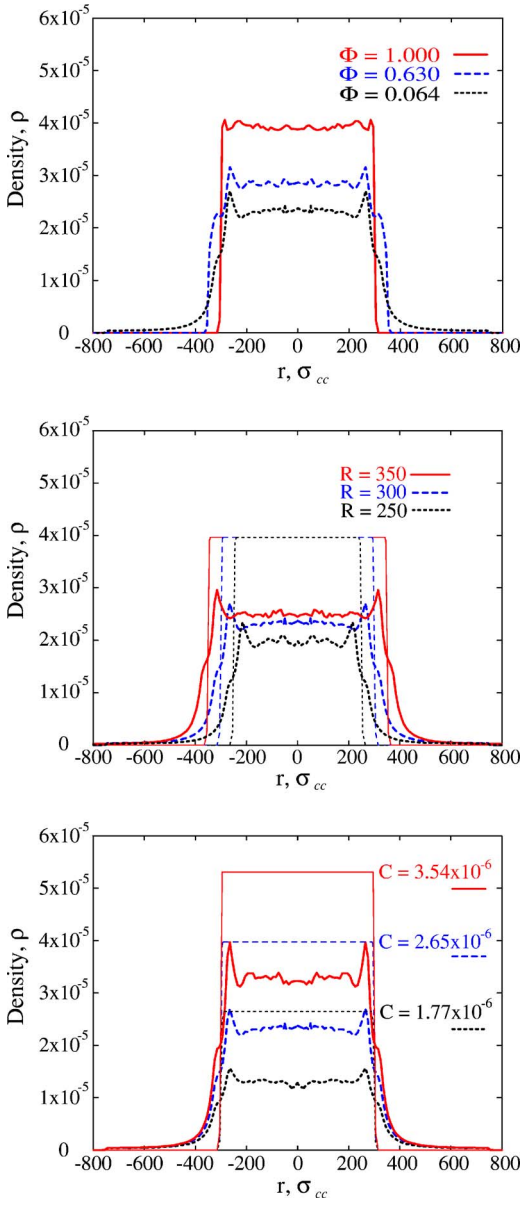

FIG. 5. (Color online) Typical density profiles of counterions across the spherical WS cell at (a) various capsule volume fractions at $R=300\sigma_{cc}$, $C=2.65\times10^{-6}$; (b) various capsule radii ($R=250$, 300, and $350\sigma_{cc}$) polyelectrolyte concentration $C=2.65\times10^{-6}$, $\Phi \sim 0.05$ is nearly the same; (c) various polyelectrolyte concentrations $C=1.77\times10^{-6}$, 2.65×10^{-6}, and 3.54×10^{-6} ($R=300\sigma_{cc}$, $\Phi=0.064$). The thin lines show the corresponding density profiles for the case $\Phi=1$.

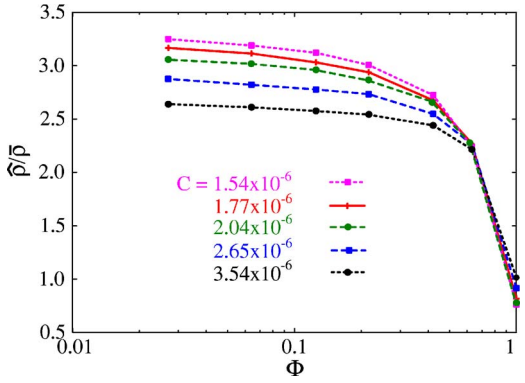

FIG. 6. (Color online) Typical ratios of mean polyelectrolyte density in the surface layer ($25\sigma_{cc}$) to the mean polyelectrolyte density in the capsule bulk as a function of capsule volume fraction Φ (capsule radius $R=300\sigma_{cc}$) for different concentrations of encapsulated polyelectrolyte, C.

The effect of various simulation parameters on the density profiles of the encapsulated polyelectrolyte is illustrated in Fig. 7. The density profile changes most dramatically upon variation of capsule volume fraction Φ. The variation of the parameter Φ controls the ionic equilibrium across the shell as well as polymer charge and thus nicely illustrates the crucial role of counterion leakage in formation of the characteristic polymer density profiles. The profile changes very significantly during transition from a neutral capsule interior ($\Phi=1$), where the polymer distribution is completely homogeneous, to the case of the lower capsule volume fraction ($\Phi \ll 1$), with noncompensated charge of the encapsulated polyelectrolyte in Fig. 7(a), with well-expressed peaks near the surface. Once again, the peaks reflect the presence of repulsive interactions between the polymer chains.

We remark and stress that there is a discernible difference in the profiles for the capsules of different radii. Thus in Fig. 7(b) the polyelectrolyte concentration in the central plateau remains constant, while the peak height increases with the capsule radius. This feature should be characteristic for nanocapsules with relatively small number of "surface" polymers. Finally, the shape of the density profiles depends on the concentration of encapsulated material. Both adsorption peaks and the height of the central plateau are getting larger with the polyelectrolyte concentration inside the capsule [see Fig. 7(c)]. Since they scale roughly linearly with the polyelectrolyte concentration the shape of the profile remains nearly constant. Another important point to note is that the height of the central plateau can be significantly smaller than would be expected in case of a uniform distribution of encapsulated polymers, so that it should not be used for an evaluation of amount of loaded materials.

IV. CONCLUSIONS

In summary, we have performed an MD simulation of charged polymer and counterion distribution in "filled" nanocapsules. To do this, we have introduced a "colloidal" model of a dilute polyelectrolyte solution. Our model led to a simple, but very accurate analysis of the spatial distribution

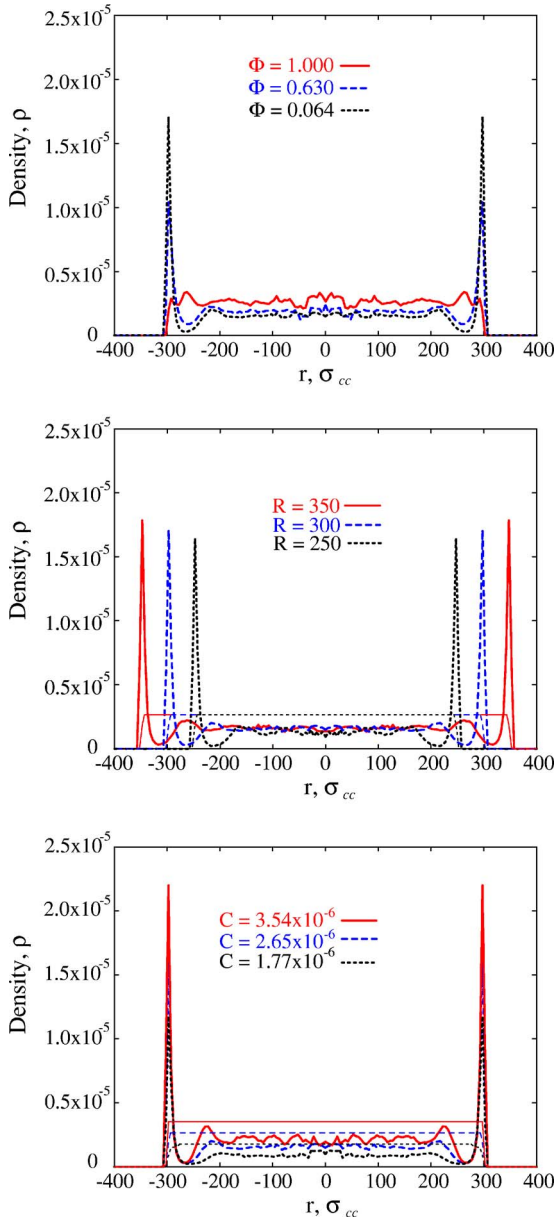

FIG. 7. (Color online) Typical density profiles of encapsulated polyelectrolyte across the capsule at (a) various capsule volume fractions at $R=300\sigma_{cc}$, $C=2.65\times10^{-6}$; (b) various capsule radii ($R=250$, 300, and $350\sigma_{cc}$) polyelectrolyte concentration $C=2.65\times10^{-6}$, $\Phi\sim0.05$ is nearly the same; (c) various polyelectrolyte concentrations $C=1.77\times10^{-6}$, 2.65×10^{-6}, and 3.54×10^{-6} ($R=300\sigma_{cc}$, $\Phi=0.064$). Thin lines show corresponding density profiles for the case $\Phi=1$.

of encapsulated materials. We have then investigated capsules of various radii and concentration of encapsulated polymer, and explored the role played by the capsule packing fraction in a dispersion. It was found that the distribution of encapsulated polymer inside the capsule is not uniform. It displays characteristic maxima near the capsule shell. These maxima were proven to appear due to the repulsive electrostatic interaction of the polyelectrolyte chains, which is shown to be a consequence of counterion leakage from the capsule interior.

ACKNOWLEDGMENTS

This work has been supported by the Alexander von Humboldt Foundation, the Deutsche Forschungsgemeinschaft, and the Russian Academy of Sciences. We are grateful to A. Y. Grosberg, M. Deserno, R. Tsekov, and B. S. Kim for stimulating discussions, and to V. A. Ivanov for helpful remarks.

[1] E. Donath, G. B. Sukhorukov, F. Caruso, S. A. Davis, and H. Möhwald, Angew. Chem., Int. Ed. **37**, 2202 (1998).
[2] G. Schneider and G. Decher, Nano Lett. **4**, 1833 (2004).
[3] G. B. Sukhorukov, A. A. Antipov, A. Voigt, E. Donath, and H. Möhwald, Macromol. Rapid Commun. **22**, 44 (2001).
[4] L. Dähne, S. Leporatti, E. Donath, and H. Möhwald, J. Am. Chem. Soc. **123**, 5431 (2001).
[5] V. V. Lulevich, I. L. Radtchenko, G. B. Sukhorukov, and O. I. Vinogradova, J. Phys. Chem. B **107**, 2735 (2003).
[6] O. I. Vinogradova, D. Andrienko, V. V. Lulevich, S. Nordschild, and G. B. Sukhorukov, Macromolecules **37**, 1113 (2004).
[7] D. V. Volodkin, N. I. Larionova, and G. B. Sukhorukov, Biomacromolecules **5**, 1962 (2004).
[8] G. B. Sukhorukov, D. G. Shchukin, W. F. Dong, H. Möhwald, V. V. Lulevich, and O. I. Vinogradova, Macromol. Chem. Phys. **205**, 530 (2004).
[9] B. S. Kim and O. I. Vinogradova, J. Phys. Chem. B **108**, 8161 (2004).
[10] O. V. Lebedeva, B. S. Kim, and O. I. Vinogradova, Langmuir **20**, 10685 (2004).
[11] O. I. Vinogradova, J. Phys.: Condens. Matter **16**, R1105 (2004).
[12] B. S. Kim, O. V. Lebedeva, K. Koynov, H. Gong, G. Glasser, I. Lieberwith, and O. I. Vinogradova, Macromolecules **38**, 5214 (2005).
[13] S. Asakura and F. Oosawa, J. Chem. Phys. **22**, 1255 (1954).
[14] A. Vrij, Pure Appl. Chem. **48**, 471 (1976).
[15] A. A. Louis, P. G. Bolhuis, J. P. Hansen, and E. J. Meijer, Phys. Rev. Lett. **85**, 2522 (2000).
[16] A. A. Louis, P. G. Bolhuis, R. Finken, V. Krakoviack, E. J. Meijer, and J. P. Hansen, Physica A **306**, 251 (2002).
[17] C. N. Likos, H. Löwen, M. Watzlawek, B. Abbas, O. Jucknischke, J. Allgaier, and D. Richter, Phys. Rev. Lett. **80**, 4450 (1998).
[18] D. Gottwald, C. N. Likos, G. Kahl, and H. Löwen, Phys. Rev. Lett. **92**, 068301 (2004).
[19] R. W. Hockney and J. W. Eastwood, *Computer Simulation Using Particles* (McGraw-Hill, New-York, 1981).
[20] M. Deserno and C. Holm, J. Chem. Phys. **109**, 7678 (1998); **109**, 7694 (1998).
[21] A. Arnold and C. Holm, Comput. Phys. Commun. **117**, 2496 (2002).
[22] H. Limbach, A. Arnold, B. Mann, and C. Holm (unpublished).
[23] P. Chu and J. A. Marinsky, J. Phys. Chem. **71**, 3884 (1967).
[24] A. Takahashi, N. Kato, and M. Nagasawa, J. Phys. Chem. **74**, 944 (1970).
[25] G. Versnaver and J. Škerjanc, J. Phys. Chem. **90**, 4673 (1986).
[26] M. Reddy and J. A. Marinsky, J. Phys. Chem. **74**, 3884 (1970).
[27] T. Odijk, J. Polym. Sci., Polym. Phys. Ed. **15**, 477 (1977).
[28] J. Skolnick and M. Fixman, Macromolecules **10**, 944 (1977).
[29] R. Klein, H. H. von Grünberg, C. Bechinger, M. Brunner, and V. Lobaskin, J. Phys.: Condens. Matter **14**, 7631 (2002).
[30] V. Lobaskin, M. Brunner, C. Bechinger, and H. H. von Grunberg, J. Phys.: Condens. Matter **15**, 6693 (2003).
[31] V. V. Lulevich, I. L. Radtchenko, G. B. Sukhorukov, and O. I. Vinogradova, Macromolecules **36**, 2832 (2003).
[32] V. Lobaskin and P. Linse, J. Chem. Phys. **111**, 4300 (1999).
[33] V. Lobaskin, B. Duenweg, and C. Holm, J. Phys.: Condens. Matter **16**, S4063 (2004).